HHS Public Access

Author manuscript

Mol Neurobiol. Author manuscript; available in PMC 2017 August 01.

Published in final edited form as:

Mol Neurobiol. 2017 August ; 54(6): 4189–4200. doi:10.1007/s12035-016-9997-9.

The Neuron-Specific Protein TMEM59L Mediates Oxidative Stress-Induced Cell Death

Qiuyang Zheng[1], **Xiaoyuan Zheng**[1], **Lishan Zhang**[1], **Hong Luo**[1], **Lingzhi Qian**[1], **Xing Fu**[1], **Yiqian Liu**[1], **Yuehong Gao**[1], **Mengxi Niu**[1], **Jian Meng**[1], **Muxian Zhang**[1], **Guojun Bu**[1], **Huaxi Xu**[1,2], and **Yun-wu Zhang**[1]

[1]Fujian Provincial Key Laboratory of Neurodegenerative Disease and Aging Research, Institute of Neuroscience, College of Medicine, Collaborative Innovation Center for Brain Science, Xiamen University, Xiamen, Fujian 361102, China

[2]Degenerative Disease Research Program, Sanford-Burnham-Prebys Medical Discovery Institute, La Jolla, CA 92037, USA

Abstract

TMEM59L is a newly identified brain-specific membrane-anchored protein with unknown functions. Herein we found that both TMEM59L and its homolog, TMEM59, are localized in Golgi and endosomes. However, in contrast to a ubiquitous and relatively stable temporal expression of TMEM59, TMEM59L expression was limited in neurons and increased during development. We also found that both TMEM59L and TMEM59 interacted with ATG5 and ATG16L1, and that overexpression of them triggered cell autophagy. However, overexpression of TMEM59L induced intrinsic caspase-dependent apoptosis more dramatically than TMEM59. In addition, downregulation of TMEM59L prevented neuronal cell death and caspase-3 activation caused by hydrogen peroxide insults and reduced the lipidation of LC3B. Finally, we found that AAV-mediated knockdown of TMEM59L in mice significantly ameliorated caspase-3 activation, increased mouse duration in the open arm during elevated plus maze test, reduced mouse immobility time during forced swim test, and enhanced mouse memory during Y-maze and Morris water maze tests. Together, our study indicates that TMEM59L is a pro-apoptotic neuronal protein involved in animal behaviors such as anxiety, depression, and memory, and that TMEM59L downregulation protects neurons against oxidative stress.

Keywords

TMEM59L; TMEM59; Apoptosis; Autophagy; Oxidative stress

Correspondence to: Yun-wu Zhang.

Electronic supplementary material The online version of this article (doi:10.1007/s12035-016-9997-9) contains supplementary material, which is available to authorized users.

Compliance with Ethical Standards

Conflict of Interest The authors declare that they have no conflict of interest.

Introduction

Cell death is a critical and active process that maintains tissue homeostasis and eliminates potentially harmful cells. There are three major types of cell death including apoptosis (also known as type I cell death), autophagy (type II), and necrosis (type III) [1]. Apoptosis can be mediated by either caspase-dependent or caspase-independent pathways [2], and caspase-dependent pathway can be further classified as extrinsic and intrinsic pathways [2, 3]. The former is stimulated by ligation of death receptors and subsequent caspase-8 activation; the latter is assumed to initiate in mitochondria, whose activation involves release of cytochrome C and subsequent activation of pro-caspase-9 [4]. Both caspase-8 and caspase-9 initiate a cascade reaction, leading the cleavage and thus activation of caspase-3 and caspase-7, and subsequent cleavage of the death substrate poly-(ADP-ribose) polymerase (PARP) [5], resulting in the execution of apoptosis in cells.

Autophagy is a catabolic process of self-degradation of bulk cytoplasmic components in which double-membrane autophagosomes sequester organelles or potions of cytosol and fuse with lysosomes for break down [6]. Autophagosome formation and maturation is regulated by the sequential function of autophagy-related (ATG) proteins, which is started with the formation of a preinitiation complex consisting of ULK1/ATG1, FIP200, and ATG13. The preinitiation complex then recruits and activates an initiation complex composing of Beclin1, Vps34, and Vps15 [7]. Membrane elongation and autophagosome closure are driven by two ubiquitin-like modification systems: the ATG5-ATG12-ATG16L1 and the LC3-PE conjugation pathways. ATG7 and ATG10 transfer ATG12 to ATG5 and then the ATG5-ATG12 conjugate recruits ATG16L1 to form a large complex [8]. On the other hand, LC3 (including LC3A and LC3B) is cleaved by ATG4. The produced LC3-I binds to ATG7 and is transferred to ATG3. The ATG5-ATG12-ATG16L1 complex then acts as an E3 ligase to conjugate LC3-I to phosphatidyl-ethanolamine (PE) [8]. LC3-PE, also known as LC3-II, is a hallmark of autophagosome formation [1, 9].

The chemical reduction-oxidation balance commands physiological and pathological responses at different levels ranging from cells to tissues to biological systems. Among organs, the brain is especially vulnerable to oxidative insults [10]. Mitochondrion is considered as the primary sources of reactive oxygen species (ROS) which account for the majority of unfavorable neural apoptosis generation [11]. Cumulative oxidative stress may induce cellular damage, impairment of the DNA repair system, and mitochondrial dysfunction, and contribute to the development of neurodegenerative disorders, such as Alzheimer’s disease, Parkinson’s disease, and Hungtinton’s disease [12]. However, the detailed mechanism underlying oxidative stress-induced neurotoxicity has not been fully elucidated.

Transmembrane protein 59-like (TMEM59L) is a brain-specific transmembrane protein [13]. Its brain-specific expression pattern implicates that TMEM59L likely plays a role in the function of the central nervous system. However, so far there is very limited information on the physiological function of TMEM59L. A recent study suggested that both TMEM59L and its homolog, TMEM59, can modulate complex N- and O-glycosylation steps occurring during the Golgi maturation of APP that is crucially involved in Alzheimer’s disease, thus

inhibiting APP transport to the cell surface and further shedding [14]. Another report found that overexpression of TMEM59L may induce apoptosis with unknown mechanism [15]. On the other hand, TMEM59 was found to contain an ATG16L1-binding motif that promotes local activation of LC3 and evokes autophagy [16]. Herein, we systematically compared the role of TMEM59L and TMEM59 in mediating cell apoptosis and autophagy. Our results demonstrate that although both TMEM59L and TMEM59 overexpression induce autophagy, TMEM59L overexpression has a much stronger effect on inducing intrinsic caspase-dependent apoptosis than TMEM59. Notably, we find that downregulation of TMEM59L ameliorates oxidative stress-caused neuronal death. Moreover, we show that downregulation of TMEM59L in mice can reduce anxiety and depression and promote memory, implying a regulatory role of TMEM59L in animal behaviors.

Materials and Methods

Antibodies and Reagents

Antibodies used were as follows: anti-cleaved caspase-3 (catalog number 9664), anti-caspase-8 (catalog number 9746), anti-caspase-9 (catalog number 9508), anti-cleaved PARP (human specific, catalog number 9546), anti-cleaved PARP (mouse specific, catalog number 9548), anti-cytochrome C (catalog number 4280), anti-COX IV (catalog number 4850), anti-GAPDH (catalog number 5174), anti-β-actin (catalog number 3700), anti-LC3B (catalog number 3868), and anti-GluR1 (catalog number 13185) from Cell Signaling Technology; anti-GluR2 (catalog number MAB397), anti-NR2A (catalog number 07-632), anti-PSD95 (catalog number MAB1596), and anti-α-tubulin (catalog number MABT205) from Merck Millipore; anti-Synaptophysin (catalog number s-5768) from Sigma-Aldrich; anti-myc antibody (catalog number sc-40) from Santa Cruz Biotechnology; anti-GFP (catalog number M20004) and anti-HA antibody (catalog number M20003) from Abmart; horseradish peroxidase (HRP)-conjugated goat anti-rabbit IgG (H + L) secondary antibody (catalog number 31460), HRP-conjugated goat anti-mouse IgG (H + L) secondary antibody (catalog number 31430), Alexa-Fluor-594-conjugated goat anti-mouse IgG (catalog number A-11005), and Alexa-Fluor-488-conjugated goat anti-rabbit IgG (catalog number A-11008) from Thermo Fisher.

Pan-caspase inhibitor Z-VAD, hydrogen peroxide, 4’,6-diamidino-2-phenylindole (DAPI), and tunicamycin were purchased from Sigma-Aldrich.

Cells Cultures

Human HEK293T cells, HEK293A cells, Hela cells, and mouse neuroblastoma N2a cells were maintained in high-glucose DMEM (Hyclone) supplemented with 10 % fetal bovine serum (FBS, Gibco), 100 units/ml penicillin (Gibco), and 100 μg/ml streptomycin (Gibco). Primary cortical neurons were prepared from embryonic day 16.5 (E16.5) mouse pups and maintained in neurobasal medium (Gibco) supplemented with 2% B27 (Gibco), 2 mM glutamine (Gibco), 100 units/ml penicillin (Gibco), and 100 μg/ml streptomycin (Gibco).

Animals

C57BL/6 mice were maintained at 12/12-h light and dark cycle with ad libitum food and water. All animal procedures were in accordance with the National Institute of Health Guidelines for the Care and Use of Laboratory Animals and were approved by the Animal Ethics Committee of Xiamen University.

DNA Constructs and Adenoviruses

Myc-tagged TMEM59L, TMEM59, and ATG3 were constructed by using the pCDNA3.1-myc/his (Invitrogen) construct as backbones. Myc-ATG5 was constructed by using the pCMV-myc (Clontech) construct as backbone; GFP-tagged TMEM59L and TMEM59 were constructed by using the pEGFP-N1 (Clontech) as backbones. HA-tagged LC3B and ATG16L1 were constructed by using the pCMV-HA (Clontech) vector as backbones. GFP-tagged Rab5 plasmid was kindly provided by Dr. Steve Caplan (University of Nebraska, Lincoln, NE); Rab7 (Addgene plasmid #12605) and Rab11 (Addgene plasmid #12674) were kindly provided by Dr. Richard Pagano (Mayo Clinic, Rochester, MN) and obtained from Addgene.

Pre-made adenoviruses encoding human *TMEM59L* cDNA fused with HA tag (Ad-59L-HA) and control adenovirus were purchased from Abmgood, and amplified in HEK293A cells and purified as described previously [17].

RNA Interference

The shRNA targeting mouse *Tmem59l* and the scrambled shRNA were constructed in the pLL3.7 vector (pLL3.7 was a gift from Luk Parijs, Addgene plasmid #11795). The sequence of the shRNA primers were as follows: scrambled sequence 5′-GCCATATGTTCGAGACTCT-3′; *Tmem59l*-shRNA1: 5′-GCTATCCTGATCAGTGCTT-3′; *Tmem59l*-shRNA2: 5′-GAGAGTGACTTCCTCAGTT-3′. The *Tmem59l*-shRNA1 sequence and a scrambled shRNA sequence (5′-TTCTCCGAACGTGTCACGT-3′) were inserted into the pAKD-CMV-bGlobin-eGFP-H1-shRNA vector for adeno-associated virus (AAV) packaging, which was serviced by Obio Technology (Shanghai, China).

Transfection and Infection

HEK293T and N2a cells were transfected with indicated plasmids using Turbofect transfection reagent (Thermo Fisher), following the manufacturer's protocol. Primary neurons were transduced with adenovirus for 4 days or AAV for 7 days before harvesting.

Quantitative Real Time-PCR (qRT-PCR)

Total RNA was extracted using the TRIzol reagent (Thermo Fisher) and then reverse transcribed into cDNA using the Rever Tra Ace qPCR RT Kit (TOYOBO). qRT-PCR reactions were performed using the FastStart Universal SYBR Green Master (ROX) (Roche) with specific primers designed for indicated target genes. β-*actin* was served as an internal control. Primers used for qRT-PCR amplification were shown in Table S1.

Western Blot

Cells or mouse brain tissues were lysed in RIPA lysis buffer (25 mM Tris-HCl, pH 7.6, 150 mM NaCl, 1 % sodium deoxycholate, 1 % Nonidet P-40, 0.1 % sodium dodecyl sulfate), supplemented with the Complete Protease Inhibitor Cocktail (Roche). Equal amounts of protein lysates were resolved on SDS-polyacrylamide gel electrophoresis, transferred to polyvinylidene difluoride (PVDF) membrane (Merck Millipore), and then blotted with indicated primary antibodies. Protein band intensity was quantified by densitometry by using the Image J software.

Mitochondrial Isolation

Mitochondria of HEK293Tcells transfected with TMEM59L-myc were isolated with a Mitochondrial Isolation Kit (Beyotime Biotechnology), following the manufacturer's protocol. Equal amounts of protein lysates of mitochondrial and cytosol fractions were subjected to Western blot analysis.

Co-immunoprecipitation

Treated HEK293T cells were lysed with TNE lysis buffer (25 mM Tris-HCl, pH 7.6, 150 mM NaCl, 1 mM EDTA, 1 % Nonidet P-40) supplied with the Complete Protease Inhibitor Cocktail (Roche). Cell lysates were subjected to immunoprecipitation with indicated antibodies and incubation with recombinant Protein G beads (Thermo Fisher). The beads were then washed with lysis buffer, mixed with sample buffer, heated, and analyzed by Western blot.

Immunofluorescence

Cells grown on coverslips in 24-well plates were fixed in 4 % paraformaldehyde saline for 15 min at room temperature, permeabilized with 0.2 % Triton X-100 in PBS for 5 min, and blocked in 5 % bovine serum albumin (BSA) for 30 min. Cells were immunostained with indicated primary antibodies at 4 °C overnight and then incubated with the fluorescence-conjugated secondary antibodies, nuclei were counterstained with DAPI. Cells were visualized under a confocal fluorescence microscope (Nikon).

Terminal Transferase dUTP Nick End Labeling (TUNEL) Assay

To identify apoptotic cells, TUNEL assays using an In Situ Cell Death Detection Kit, TMR red (Roche) were performed following the manufacturer's protocol and counterstained with DAPI. Positively stained cells were scored in five randomized fields under a fluorescent microscope.

Stereotactic Injection

AAV-sc-shRNA and AAV-59l-shRNA (viral titer 8.7×10^{12}) were stereotactically injected into the two lateral ventricles of wild-type C57BL/6 postnatal day 0 (P0) neonates. Two months after injection, mice were used for behavioral tests and then sacrificed for biochemical analyses.

Behavioral Tests

Experimental mice injected with AAVs were subjected to open field test, elevated plus maze test, forced swim test, social interaction test, Y-maze test, and Morris water maze test. Test details were provided in Supplemental Materials and Methods.

Statistical Analysis

Statistical analyses were performed with Graphpad Prism. Differences between two means were assessed by unpaired *t* tests. Differences among multiple means were assessed by ANOVAs. All data were presented as mean ± s.e.m.

Results

Expression Patterns of TMEM59L and Its Homolog TMEM59

Sequence alignment revealed that TMEM59L protein sequences highly conserved among different species from human to zebra fish, and the identity between human and mouse TMEM59L is 75 % (Fig. S1a). Both TMEM59L and its homolog TMEM59 are type I transmembrane proteins (predicted by TMHMM Server v.2.0) that share 28.3 % identity (Fig. S1b). To examine the expression pattern of TMME59L and TMEM59, we compared the messenger RNA (mRNA) levels in different neural cell types. We found that TMEM59L was highly specifically expressed in neurons, but not in astrocytes and microglia (Fig. 1a). In addition, we confirmed that TMEM59L was preferentially expressed in the mouse brain including cerebral cortex, cerebellum, and hippocampus regions (Fig. 1b). In contrast, TMEM59 was ubiquitously expressed in all three neural cell types (Fig. 1a), as well as in various mouse tissues (Fig. 1b). In addition, we found that TMEM59L expression was detected in the brain early at embryonic day 8.5 (E8.5), and increased until to 3 month of age, whereas the expression of TMEM59 was relatively low and stable at different development stages (Fig. 1c). The pattern of TMEM59L expression implicates that TMEM59L likely plays an important role in neural development, which deserves further scrutiny.

Furthermore, we examined subcellular localizations of TMEM59L and TMEM59. Immunofluorescence analysis showed that both TMEM59L and TMEM59 were partially colocalized with the early endosome marker Rab5 (Fig. 1d), the late endosome marker Rab7 (Fig. 1e), the recycling endosome marker Rab11 (Fig. 1f), and the cis-Golgi marker Giantin (Fig. 1g). These results are consistent with previous studies showing a Golgi localization of both TMEM59L and TMEM59 [14], and an endosome localization of TMEM59 [16].

In addition, NetNGlyc 1.0 Server predicted that both TMEM59L and TMEM59 had one potential N-linked glycosylation site (N97 in TMEM59L and N90 in TMEM59) (Fig. S1). Treatment of TMEM59L and TMEM59 overexpressing cells with tunicamycin, a general N-glycosylation inhibitor, produced faster migrating and more compact TMEM59L and TMEM59 protein bands in Western blots, indicating their N-glycosylation. When their putative glycosylated sites were mutated into non-glycosylated amino acids (N97Q in TMEM59L and N90Q in TMEM59), there were no more changes in their molecular weights

after tunicamycin treatment (Fig. S3), suggesting that both of TMEM59L and TMEM59 were modestly N-glycosylated proteins.

Overexpression of TMEM59L Induces Intrinsic Caspase-Dependent Apoptosis More Dramatically than Overexpression of TMEM59

A study found that overexpression of TMEM59L may induce apoptosis [15]. But the underlying mechanism remains elusive. To dissect the pro-apoptotic activity of TMEM59L, we overexpressed TMEM59L in HEK293T cells and found a significant increase in the level of apoptosis as determined by TUNEL staining (Fig. 2a, b). In addition, we found that overexpression of TMEM59 also induced cell apoptosis, but to a much weaker extent when compared to TMEM59L overexpression (Fig. 2a, b). Moreover, we found that overexpression of TMEM59L resulted in dramatic cleavage (activation) of caspase-3, as well as cleavage of PARP which indicated the activation of caspases in both HEK293T and N2a cells (Fig. 2c, d). In contrast, overexpression of TMEM59 had marginal effect on inducing the cleavage of caspase-3 and PARP (Fig. 2c, d). In addition, primary cortical neurons infected with adenovirus expressing TMEM59L resulted in a robust activation of caspase-3 and cleavage of PARP (Fig. 2e), indicating that TMEM59L upregulation can induce neuronal apoptosis. Together, these results demonstrate that TMEM59L is a strong pro-apoptotic protein.

Caspase-dependent pathways can be classified as intrinsic or extrinsic and are primarily associated with caspase-9 or caspase-8, respectively, both of which activate caspase-7 and caspase-3 at later stages [2]. We further investigated the exact pathway involved in TMEM59L-induced apoptosis and found that overexpression of TMEM59L induced cleavage of caspase-9 but not caspase-8 (Fig. 2f). Moreover, we found that overexpression of TMEM59L resulted in release of cytochrome C from mitochondria into the cytosol (Fig. 2g). When cells were treated with Z-VAD, a pan-caspase inhibitor, the cleavage of caspase-3 and the cleavage of PARP were significantly reduced (Fig. 2h). The TUNEL staining result also showed that Z-VAD treatment alleviated apoptosis induced by TMEM59L overexpression (Fig. 2i, j), implicating that caspase activity was indispensable for TMEM59L-mediated apoptosis. Together, these data suggest that TMEM59L induces apoptosis through the caspase-dependent intrinsic pathway.

Both TMEM59L and TMEM59 Interact with ATG5 and ATG16L1 and Their Overexpression Induces Autophagy

TMEM59 has an ATG16L1 binding motif which can promote LC3 activation and mediate autophagy in response to *Staphylococcus aureus* infection [16]. Herein, we found that similar to overexpression of TMEM59, overexpression of TMEM59L also significantly enhanced LC3B lipidation indicated by the increased level of LC3B-II (Fig. 3a, b), suggesting the activation of autophagy. In addition, the level of LC3B-II was markedly increased in primary cortical neurons infected with adenovirus expressing TMEM59L (Fig. 3c, d). Moreover, we found that overexpression of both TMEM59L and TMEM59 induced HA-LC3B redistribution to vesicular structures (Fig. 3e, f). Taken together, these data indicate that overexpression of both TMEM59L and TMEM59 can induce autophagy.

Since TMEM59 has been found to interact with ATG16L1 [16], we also studied and indeed found that TMEM59L can also interact with ATG16L1 (Fig. 3g). Moreover, we explored potential interaction of TMEM59L and TMEM59 with other autophagy machinery proteins. Our results identified that both TMEM59L and TMEM59 interacted with ATG5 (Fig. 3h), but not with ULK1 (Fig. S2a, b) or ATG3 (Fig. S2c).

Downregulation of TMEM59L Protects Neuronal Cells Against Hydrogen Peroxide Insult

Neuronal cells are susceptible to acute oxidative stress [18]. To study whether the pro-apoptotic TMEM59L contributes to oxidative stress-induced cell death, we treated mouse primary cortical neurons with hydrogen peroxide and found that the mRNA levels of *Tmem59l* were upregulated upon administration of hydrogen peroxide (Fig. S4). When we downregulated the expression of *Tmem59l* by shRNA in N2a cells (Fig. 4a), we found that both LC-3B lipidation (Fig. 4b, d) and the cleavage of caspase-3 and PARP (Fig. 4c, e, f) were significantly decreased, indicating a reduction of basal autophagy and apoptosis. In addition, when these cells were further treated with hydrogen peroxide, we found that downregulation of *Tmem59l* also dramatically reduced the cleavage of caspase-3 and PARP (Fig. 4c, e, f). TUNEL staining also confirmed that downregulation of *Tmem59l* alleviated apoptosis induced by hydrogen peroxide insult (Fig. 4g,h).

To further confirm the protection of TMEM59L downregulation against oxidative stress-induced toxicity, we generated AAV containing a shRNA sequence targeting mouse *Tmem59l* (AAV-59l-shRNA, Fig. 5a). When mouse primary cortical neurons were infected with control AAV (AAV-sc-shRNA) or AAV-59l-shRNA for 7 days to downregulate *Tmem59l* (Fig. 5b), the cleavage of caspase-3 and PARP was significantly reduced (Fig. 5c, d). Moreover, knockdown of *Tmem59l* dramatically alleviated the activation of caspase-3 and cleavage of PARP upon hydrogen peroxide insults in primary cortical neurons (Fig. 5c, d). By contrast, downregulation of *Tmem59l* did not affect the levels of glutamate receptor subunits including GluR1, GluR2 and NR2A, and synaptic components including PSD95 and synaptophysin (Fig. 5c, d). Together, these data demonstrate that downregulation of TMEM59L can protect neuronal cells against oxidative stress-induced cell death.

AAV-Mediated Knockdown of TMEM59L Reduces Anxiety- and Depressive-Like Behaviors and Enhances Memory in Mice

A neuron-specific expression pattern of TMEM59L implies its function in the central nervous system. To study this, we injected AAV-59l-shRNA or its control AAV-sc-shRNA bilaterally into the cerebral ventricle of P0 neonates of wild-type C57BL/6 mice (Fig. 6a). At 3 months after injection, the expression of GFP for indicating viral infection was evaluated in mouse brain sections. We found that intracranial delivery of AAV-59l-shRNA or AAV-sc-shRNA to neonatal mice resulted in an extensive transduction and GFP expression throughout the brain, with intensities more profound in hippocampus, cerebral cortex, and cerebellum regions (Fig. 6b). We also confirmed the reduction of *Tmem59l* expression in hippocampus, cerebral cortex, cerebellum, and hypothalamus (Fig. 6c). Furthermore, downregulation of *Tmem59l* resulted in reduced caspase-3 cleavage in the hippocampus, without alteration of glutamate receptor subunits including GluR1, GluR2, and NR2A, as well as PSD95 and synaptophysin (Fig. 6d, e). Moreover, downregulation of *Tmem59l* did

not affect synaptophsin and PSD95 distribution in synaptosome and post-synaptic density fractions (Fig. S5).

At 2 months after AAV infection, we compared various behaviors in *Tmem59l*-downregulated mice and control mice. Using an open field test to investigate locomotor activity, we found no differences in total distance of movements and time spent in the center region of the open field (Fig. 7a, b). In the elevated plus maze test, we found that *Tmem59l*-downregulated mice showed no difference of the total movement distance (Fig. 7c) but significantly increased time spent in the open arm (Fig. 7d) when compared to control mice, indicating a reduced anxiety-like behavior. In forced swim test, *Tmem59l*-downregulated mice had less immobility than control mice (Fig. 7e), suggesting a reduced depressive-like behavior. Moreover, downregulation of *Tmem59l* did not affect their social affinity and social preference (Fig. S6).

We also studied animal learning and memory. In the Y-maze test, we found that *Tmem59l*-downregulated mice had no differences for total movement distance (Fig. 7f) and total arm entries (Fig. 7g) but significantly increase alternation triplets (Fig. 7h) when compared to controls mice, suggesting an enhanced working memory. In addition, in Morris water maze test, although *Tmem59l*-downregulated mice showed no differences of total swim distance (Fig. 7i), swim speed (Fig. 7j), and escape latency during a 7-day training (Fig. 7k), these mice spent significantly increased time in the target quadrant (Fig. 7l) and crossings of the platform location (Fig. 7m). Together, these results suggest that downregulation of *Tmem59l* promotes animal memory.

Discussion

Apoptosis, naturally occurring during neuronal death, is essential for normal development and tissue homeostasis and as a defense against pathogens [19]. Dysregulation of apoptosis can impair neuronal functions. Neuronal cells are susceptible to acute oxidative insults [18], chronically elevated exposure of neurons to ROS including hydrogen peroxide leads to apoptosis contributing to many neurological disorders, such as Alzheimer's disease, Parkinson's disease, Huntington's disease, and ischemic stroke [12, 20]. Herein, we identified that the type I transmembrane protein TMEM59L was specifically expressed in neurons but not in astrocytes and microglia (Fig. 1a). In contrast to TMEM59L, its homolog TMEM59 was ubiquitously expressed in all neuronal types (Fig. 1a). TMEM59L overexpression induced caspase-dependent intrinsic apoptosis more dramatically than TMEM59 overexpression (Fig. 2). Therefore, a dysregulation of TMEM59L may contribute to oxidative stress-induced neuronal death and thus the pathogenesis of neurological disorders. Indeed, we found that hydrogen peroxide treatment not only induced caspase-3 activation and cell death in neuronal cells (Figs. 4 and 5), but also upregulated *Tmem59l* expression (Fig. S4). Importantly, downregulation of *Tmem59l* attenuated the activation of caspase-3 and cell death resulted from hydrogen peroxide insults (Figs. 4 and 5). These results suggest that TMEM59L may be a potential target for ameliorating oxidative stress-induced neurotoxicity.

Autophagy is another type of cell death [1]. TMEM59 has been reported to interact with ATG16L1 through a novel binding motif resident in its carbonyl terminus and activate LC3 [16]. Intriguingly, we found that although there was no sequence similarity found in the carbonyl terminus between TMEM59L and TMEM59 (Fig. S1b), both overexpression of TMEM59L and TMEM59 induced the lipidation of LC3B for its activation (Fig. 3a – f). In addition, downregulation of *Tmem59l* alleviated the lipidation of LC3B (Fig. 4b, d). These results indicate that TMEM59L also mediates autophagy. Moreover, we found that both TMEM59L and TMEM59 interacted with ATG16L1 and ATG5 (Fig. 3g, h), but not with ULK1 and ATG3 (Fig. S2).Therefore, TMEM59L and TMEM59 probably contribute to autophagy through regulating the formation or function of the ATG5-ATG12-ATG16L1 complex.

Genetic and biochemical studies implicate that activation of pro-apoptotic caspases plays a vital role in neural development [21–23]. During embryonic development, the nervous system is sculpted by neuronal apoptosis and excessive neurons are removed to ensure proper and precise pre- and postsynaptic connections [24]. Establishment of proper connections in the developing brain is essential for perception, language, thought, consciousness, learning, and memory [25]. The activation of caspase-3 has been found to be important for local pruning of dendrites and spines [26]. Caspase-3 deficiency can prevent the internalization of AMPA receptor and result in the reduction of long-term depression [27], which is required for memory extinction [28–30]. In the present study, we found that downregulation of *Tmem59l* in mice alleviated the activation of caspase-3 (Fig. 6d, e), reduced anxiety- and depressive-like behaviors, and enhanced memory (Fig. 7). Together, these findings indicate that one physiological function of TMEM59L is to regulate animal behaviors through controlling caspase activation cascade and apoptosis, and the detailed underlying mechanism deserves further scrutiny.

Supplementary Material

Refer to Web version on PubMed Central for supplementary material.

Acknowledgments

This work was supported in part by grants from National Natural Science Foundation of China (Nos. 81225008, 81161120496, 91332112, 91332114 and U1405222), National Institutes of Health (R01AG021173, R01AG038710, R01AG044420, and R01NS046673), Alzheimer's Association, Fujian Provincial Department of Science and Technology (2015Y4008), and Xiamen University President Fund (20720150170).

References

1. Green DR, Llambi F. Cell death signaling. Cold Spring Harbor perspectives in biology. 2015; 7(12)
2. Hail N Jr, Carter BZ, Konopleva M, Andreeff M. Apoptosis effector mechanisms: a requiem performed in different keys. Apoptosis. 2006; 11(6):889–904. [PubMed: 16547589]
3. Rust C, Gores GJ. Apoptosis and liver disease. Am J Med. 2000; 108(7):567–574. [PubMed: 10806286]
4. Caroppi P, Sinibaldi F, Fiorucci L, Santucci R. Apoptosis and human diseases: mitochondrion damage and lethal role of released cytochrome C as proapoptotic protein. Curr Med Chem. 2009; 16(31):4058–4065. [PubMed: 19754424]

5. van Wijk SJ, Hageman GJ. Poly(ADP-ribose) polymerase-1 mediated caspase-independent cell death after ischemia/reperfusion. Free Radic Biol Med. 2005; 39(1):81–90. [PubMed: 15925280]
6. Mizushima N, Komatsu M. Autophagy: renovation of cells and tissues. Cell. 2011; 147(4):728–741. [PubMed: 22078875]
7. He C, Klionsky DJ. Regulation mechanisms and signaling pathways of autophagy. Annu Rev Genet. 2009; 43:67–93. [PubMed: 19653858]
8. Hanada T, Noda NN, Satomi Y, Ichimura Y, Fujioka Y, Takao T, Inagaki F, Ohsumi Y. The Atg12-Atg5 conjugate has a novel E3-like activity for protein lipidation in autophagy. J Biol Chem. 2007; 282(52):37298–37302. [PubMed: 17986448]
9. Galluzzi L, Pietrocola F, Levine B, Kroemer G. Metabolic control of autophagy. Cell. 2014; 159(6): 1263–1276. [PubMed: 25480292]
10. Wilson C, Gonzalez-Billault C. Regulation of cytoskeletal dynamics by redox signaling and oxidative stress: implications for neuronal development and trafficking. Front Cell Neurosci. 2015; 9:381. [PubMed: 26483635]
11. Blesa J, Trigo-Damas I, Quiroga-Varela A, Jackson-Lewis VR. Oxidative stress and Parkinson's disease. Front Neuroanat. 2015; 9:91. [PubMed: 26217195]
12. Kim GH, Kim JE, Rhie SJ, Yoon S. The role of oxidative stress in neurodegenerative diseases. Exp Neurobiol. 2015; 24(4):325–340. [PubMed: 26713080]
13. Elson GC, de Coignac AB, Aubry JP, Delneste Y, Magistrelli G, Holzwarth J, Bonnefoy JY, Gauchat JF. BSMAP, a novel protein expressed specifically in the brain whose gene is localized on chromosome 19p12. Biochem Biophys Res Commun. 1999; 264(1):55–62. [PubMed: 10527841]
14. Ullrich S, Munch A, Neumann S, Kremmer E, Tatzelt J, Lichtenthaler SF. The novel membrane protein TMEM59 modulates complex glycosylation, cell surface expression, and secretion of the amyloid precursor protein. J Biol Chem. 2010; 285(27):20664–20674. [PubMed: 20427278]
15. Mannherz O, Mertens D, Hahn M, Lichter P. Functional screening for proapoptotic genes by reverse transfection cell array technology. Genomics. 2006; 87(5):665–672. [PubMed: 16503394]
16. Boada-Romero E, Letek M, Fleischer A, Pallauf K, Ramon-Barros C, Pimentel-Muinos FX. TMEM59 defines a novel ATG16L1-binding motif that promotes local activation of LC3. EMBO J. 2013; 32(4):566–582. [PubMed: 23376921]
17. Luo J, Deng ZL, Luo X, Tang N, Song WX, Chen J, Sharff KA, Luu HH, et al. A protocol for rapid generation of recombinant adenoviruses using the AdEasy system. Nat Protoc. 2007; 2(5):1236–1247. [PubMed: 17546019]
18. Ischiropoulos H, Beckman JS. Oxidative stress and nitration in neurodegeneration: cause, effect, or association? J Clin Invest. 2003; 111(2):163–169. [PubMed: 12531868]
19. Kajta M. Apoptosis in the central nervous system: mechanisms and protective strategies. Pol J Pharmacol. 2004; 56(6):689–700. [PubMed: 15662081]
20. Manzanero S, Santro T, Arumugam TV. Neuronal oxidative stress in acute ischemic stroke: sources and contribution to cell injury. Neurochem Int. 2013; 62(5):712–718. [PubMed: 23201332]
21. Cusack CL, Swahari V, Hampton Henley W, Michael Ramsey J, Deshmukh M. Distinct pathways mediate axon degeneration during apoptosis and axon-specific pruning. Nat Commun. 2013; 4:1876. [PubMed: 23695670]
22. Nikolaev A, McLaughlin T, O'Leary DD, Tessier-Lavigne M. APP binds DR6 to trigger axon pruning and neuron death via distinct caspases. Nature. 2009; 457(7232):981–989. [PubMed: 19225519]
23. Simon DJ, Weimer RM, McLaughlin T, Kallop D, Stanger K, Yang J, O'Leary DD, Hannoush RN, et al. A caspase cascade regulating developmental axon degeneration. J Neurosci. 2012; 32(49): 17540–17553. [PubMed: 23223278]
24. Yuan J, Lipinski M, Degterev A. Diversity in the mechanisms of neuronal cell death. Neuron. 2003; 40(2):401–413. [PubMed: 14556717]
25. Riccomagno MM, Kolodkin AL. Sculpting neural circuits by axon and dendrite pruning. Annu Rev Cell Dev Biol. 2015; 31:779–805. [PubMed: 26436703]
26. Erturk A, Wang Y, Sheng M. Local pruning of dendrites and spines by caspase-3-dependent and proteasome-limited mechanisms. J Neurosci. 2014; 34(5):1672–1688. [PubMed: 24478350]

27. Li Z, Jo J, Jia JM, Lo SC, Whitcomb DJ, Jiao S, Cho K, Sheng M. Caspase-3 activation via mitochondria is required for longterm depression and AMPA receptor internalization. Cell. 2010; 141(5):859–871. [PubMed: 20510932]

28. Dalton GL, Wang YT, Floresco SB, Phillips AG. Disruption of AMPA receptor endocytosis impairs the extinction, but not acquisition of learned fear. Neuropsychopharmacology. 2008; 33(10):2416–2426. [PubMed: 18046303]

29. Kim J, Lee S, Park K, Hong I, Song B, Son G, Park H, Kim WR, et al. Amygdala depotentiation and fear extinction. Proc Natl Acad Sci U S A. 2007; 104(52):20955–20960. [PubMed: 18165656]

30. Lee HK, Barbarosie M, Kameyama K, Bear MF, Huganir RL. Regulation of distinct AMPA receptor phosphorylation sites during bidirectional synaptic plasticity. Nature. 2000; 405(6789): 955–959. [PubMed: 10879537]

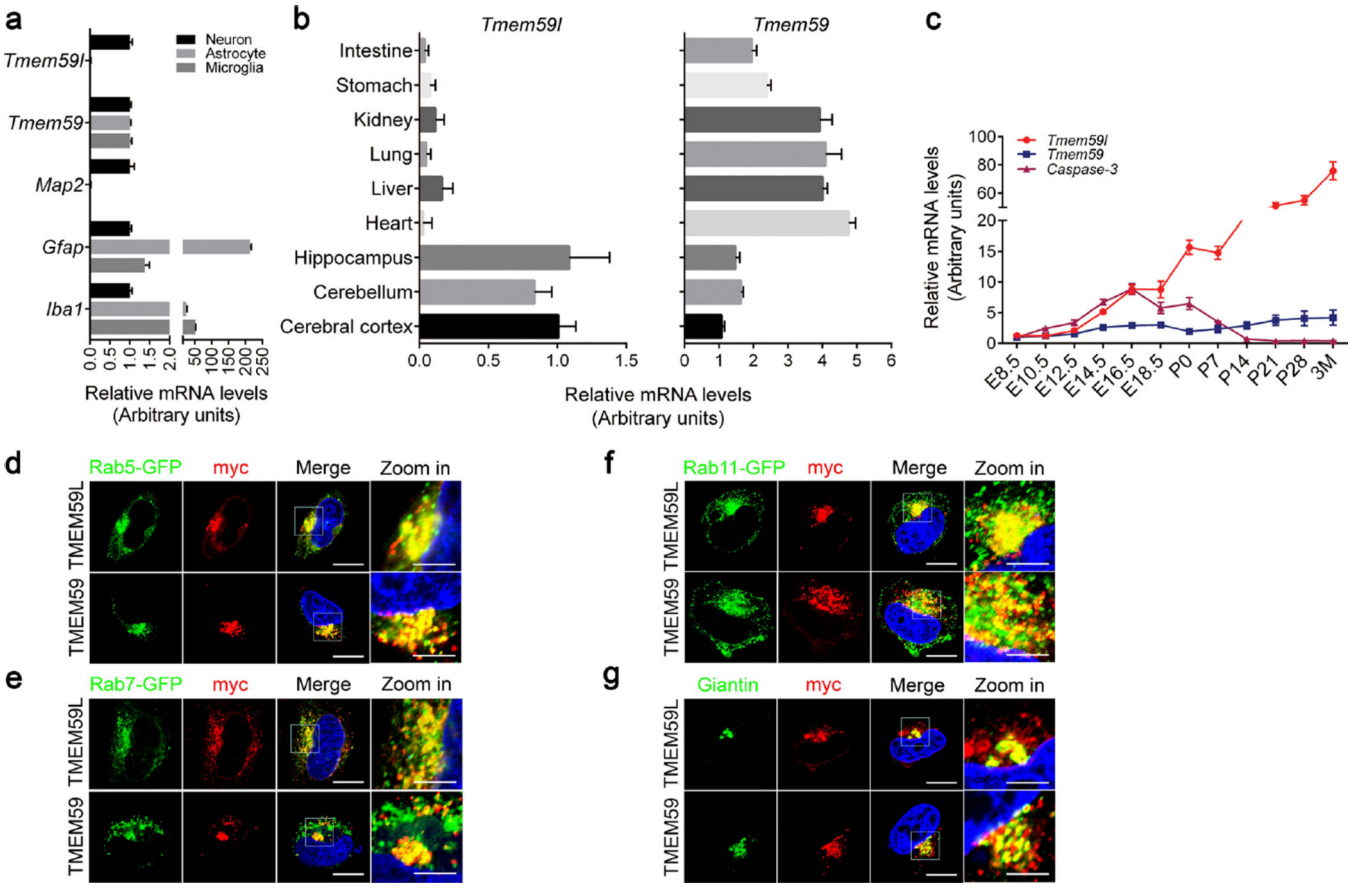

Fig. 1.

Expression pattern and subcellular localization of TMEM59L and TMEM59. **a** Total RNAs were extracted from cultured mouse primary neurons, astrocytes, and microglia, reverse transcribed, and subjected to quantitative real time-PCR (qRT-PCR). The mRNA levels of *Tmem59l*, *Tmem59*, *Map2* (neuron marker), *Gfap* (astrocyte marker), and *Iba1* (microglia marker) were normalized to those of β-*actin* and compared to those of neurons (set as one arbitrary units), $n = 3$. **b** The mRNA levels of *Tmem59l* and *Tmem59* in various mouse tissues from wild-type C57BL/6 postnatal day 0 (P0) neonates were determined by qRT-PCR, normalized to those of β-*actin*, and compared to those of cerebral cortex (set as one arbitrary units), $n = 3$. **c** The mRNA levels of *Tmem59l*, *Tmem59*, and *Caspase-3* in whole brain (E8.5-E12.5) or cerebral cortex (E14.5-3M) of wild-type C57BL/6 mice at different developmental stages were analyzed by qRT-PCR, normalized to those of β-*actin* and compared to that of E8.5 (set as one arbitrary unit), $n = 3$. **d–f** Myc-tagged TMEM59L or TMEM59 were co-transfected with GFP-tagged Rab5 (**d**, early endosome marker), Rab7 (**e**, late endosome marker), or Rab11 (**f**, recycling endosome marker) into Hela cells for 24 h. Cells were permeabilized, immunostained with mouse anti-myc antibody, incubated with a secondary goat anti-mouse IgG antibody conjugated with Alexa Fluor 594, and counterstained with DAPI, and then observed under a confocal microscope. *Red* indicates TMEM59L or TMEM59, *green* indicates GFP-tagged Rab proteins. *Blue* indicates nuclei. *Scale bars*, 10 μm ("zoom in" images); 20 μm (all other images). **g** Myc-tagged TMEM59L or TMEM59 were transfected into Hela cells for 24 h. Cells were permeabilized,

immunostained with mouse anti-myc and rabbit anti-Giantin antibodies, incubated with a secondary goat anti-mouse IgG conjugated with Alexa Fluor 594 and a second goat anti-rabbit IgG antibody conjugated with Alexa Fluor 488, counterstained with DAPI, and then observed under a confocal microscope. *Red* indicates TMEM59L or TMEM59, *green* indicates Giantin (cis-Golgi marker). *Blue* indicates nuclei. *Scale bars*: 10 μm ("zoom in" images); 20 μm (all other images)

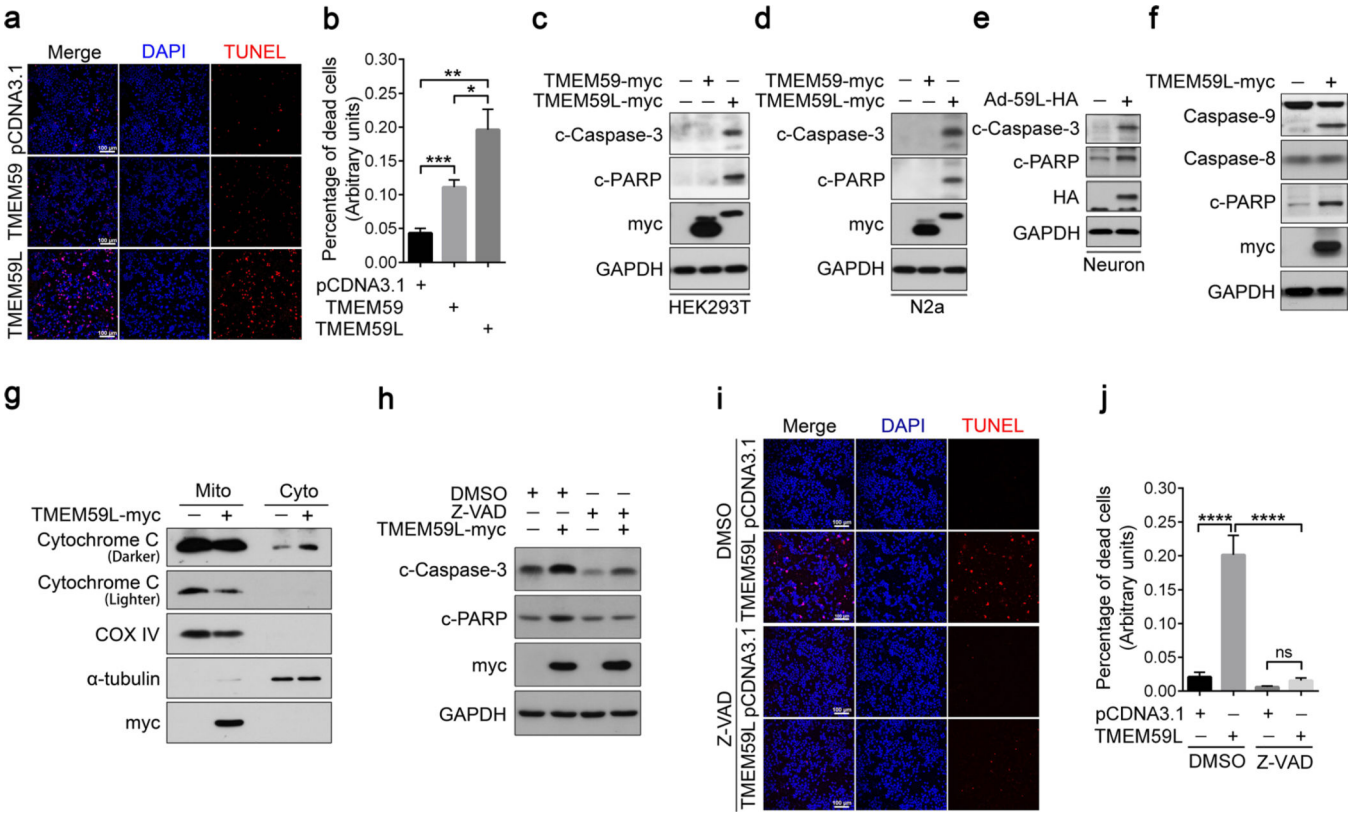

Fig. 2.

Overexpression of TMEM59L induces intrinsic caspase-dependent apoptosis more dramatically than overexpression of TMEM59. **a–c** HEK293T cells were transfected with TMEM59-myc, TMEM59L-myc, or pcDNA3.1control plasmids for 36 h. **a** Cells were stained by using Terminal transferased UTP nick end labeling (*TUNEL*) method and counterstained with DAPI. *Scale bars*, 100 μm. **b** TUNEL-positive cells were counted as apoptotic cells for comparison. $*p < 0.05$, $**p < 0.01$, $***p < 0.001$. **c** Equal amounts of protein lysates of transfected cells were subjected to Western blot for cleaved PARP (*c-PARP*) and cleaved (active) caspase-3 (*c-Caspase-3*). GAPDH was used as a loading control. **d** N2a cells were transfected with TMEM59-myc, TMEM59L-myc, or control vectors for 36 h. Cell lysates were subjected to Western blot for c-PARP and c-Caspase-3. **e** Mouse primary cortical neurons were transduced with control adenoviruses (−) or adenoviruses expressing TMEM59L (Ad-59L-HA, +). Cells were harvested after 4 days. Equal amounts of protein lysates were subjected to Western blot for c-Caspase-3 and c-PARP. **e, f** HEK293T cells were transfected with myc-tagged TMEM59L (+) or control vector (−) for 36 h. **e** Cell lysates were subjected to Western blot for caspase-9, caspase-8, and c-PARP. **f** Cells were fractionated into mitochondria (*Mito*) and cytosol (*Cyto*) fractions. Equal amounts of protein lysates were subjected to Western blot for myc, Cytochrome C, COX IV (indicative of mitochondria), and α-tubulin (indicative of the cytosol). **g–i** HEK293T cells were transfected with myc-tagged TMEM59L (+) or control vector (−) for 6 h and then treated with 50 μM Z-VAD for 30 h. **g** Cell lysates were subjected to Western blot for c-Caspase-3 and c-PARP. **h** Cells were stained by using TUNEL method and counterstained

with DAPI. *Scale bars*, 100 μm. **i** TUNEL-positive cells were counted as apoptotic cells for comparison. ns, not significant, ****$p < 0.0001$

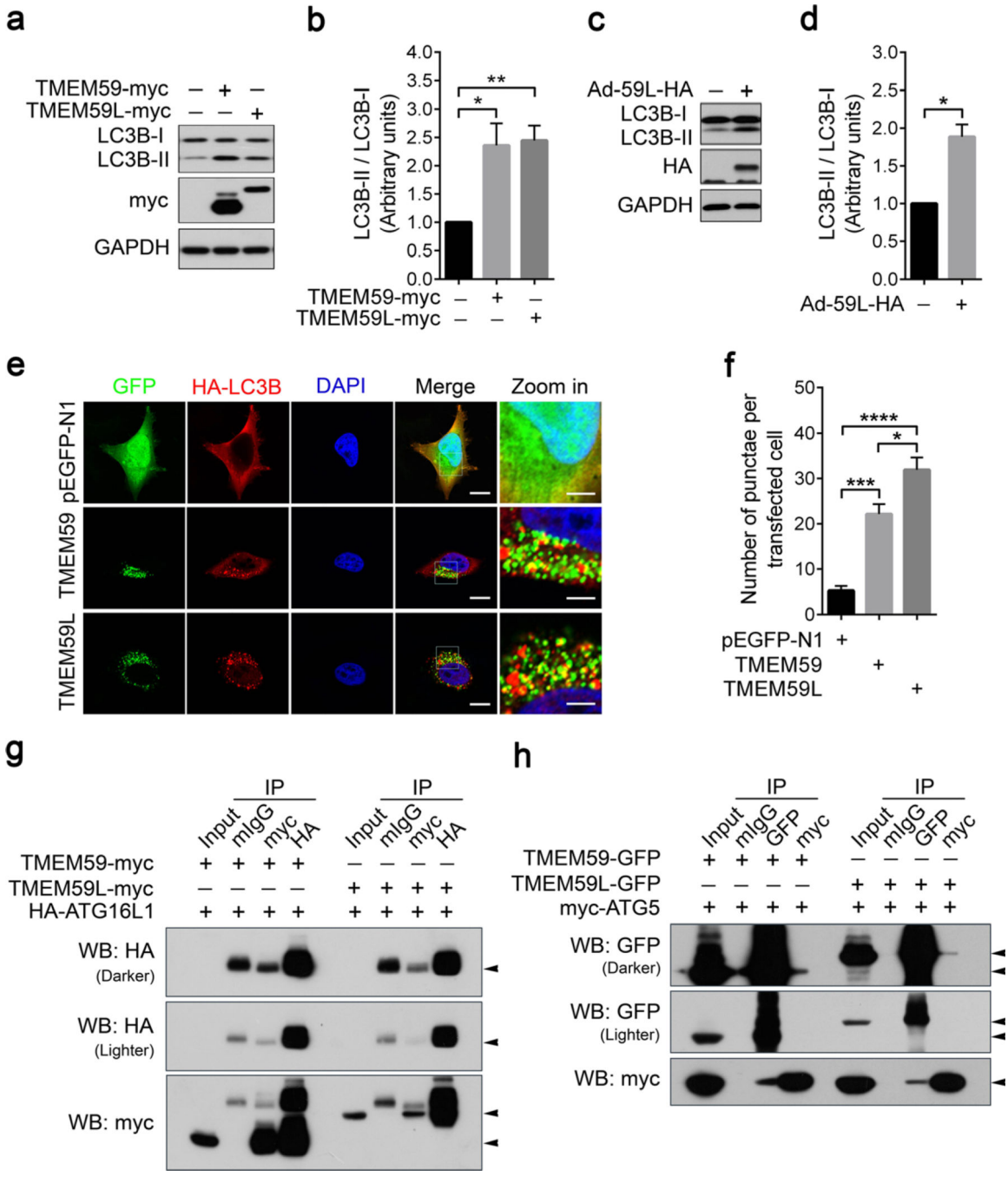

Fig. 3.

Both TMEM59L and TMEM59 interact with ATG5 and ATG16L1 and their overexpression induces autophagy. **a, b** HEK293T cells were transfected with TMEM59-myc, TMEM59L-myc, and control vector for 36 h. **a** Equal amounts of protein lysates were subjected to Western blot for LC3B-I/II. **b** Protein levels of LC3B-I and LC3B-II were quantified by using densitometry and normalized to those of GAPDH for comparison. $n = 3$, $^{*}p < 0.05$, $^{**}p < 0.01$. **c, d** Mouse primary cortical neurons were transduced with control adenoviruses (−) or adenoviruses expressing TMEM59L (Ad-59L-HA, +). Cells were harvested after 4

days. **c** Equal amounts of protein lysates were subjected to Western blot for LC3B-I/II. **d** Protein levels of LC3B-I and LC3B-II were quantified by using densitometry and normalized to those of GAPDH for comparison. $n = 3$, $^{*}p < 0.05$. **e, f** Hela cells were co-transfected with TMEM59-GFP or TMEM59L-GFP and HA-LC3B for 24 h. **e** After immunostaining with anti-HA antibody and incubating with secondary antibody, cells were observed under a confocal microscope. *Red* indicates HA-LC3B, *green* indicates GFP, and *blue* indicates nuclei. *Scale bars*: 10 μm (“zoom in” images); 20 μm (all other images). **f** The number of HA-LC3B-positive vesicles per transfected cell was counted for at least ten cells. $n = 3$,$^{*}p < 0.05$, $^{***}p < 0.001$, $^{****}p < 0.0001$. **g** Myc-tagged TMEM59 and TMEM59L were co-transfected with HA-tagged ATG16L1 into HEK293T cells. Equal amounts of cell lysates were subjected to immunoprecipitation (*IP*) with mouse normal IgG (*mIgG*), mouse antibody against myc, or mouse antibody against HA, followed by Western blot (*WB*) analysis. **h** GFP-tagged TMEM59 and TMEM59L were co-transfected with myc-tagged ATG5 into HEK293T cells. Equal amounts of cell lysates were subjected to IP with mIgG, mouse antibody against GFP, or mouse antibody against myc, followed by WB analysis. Five percent of cell lysates were used as input

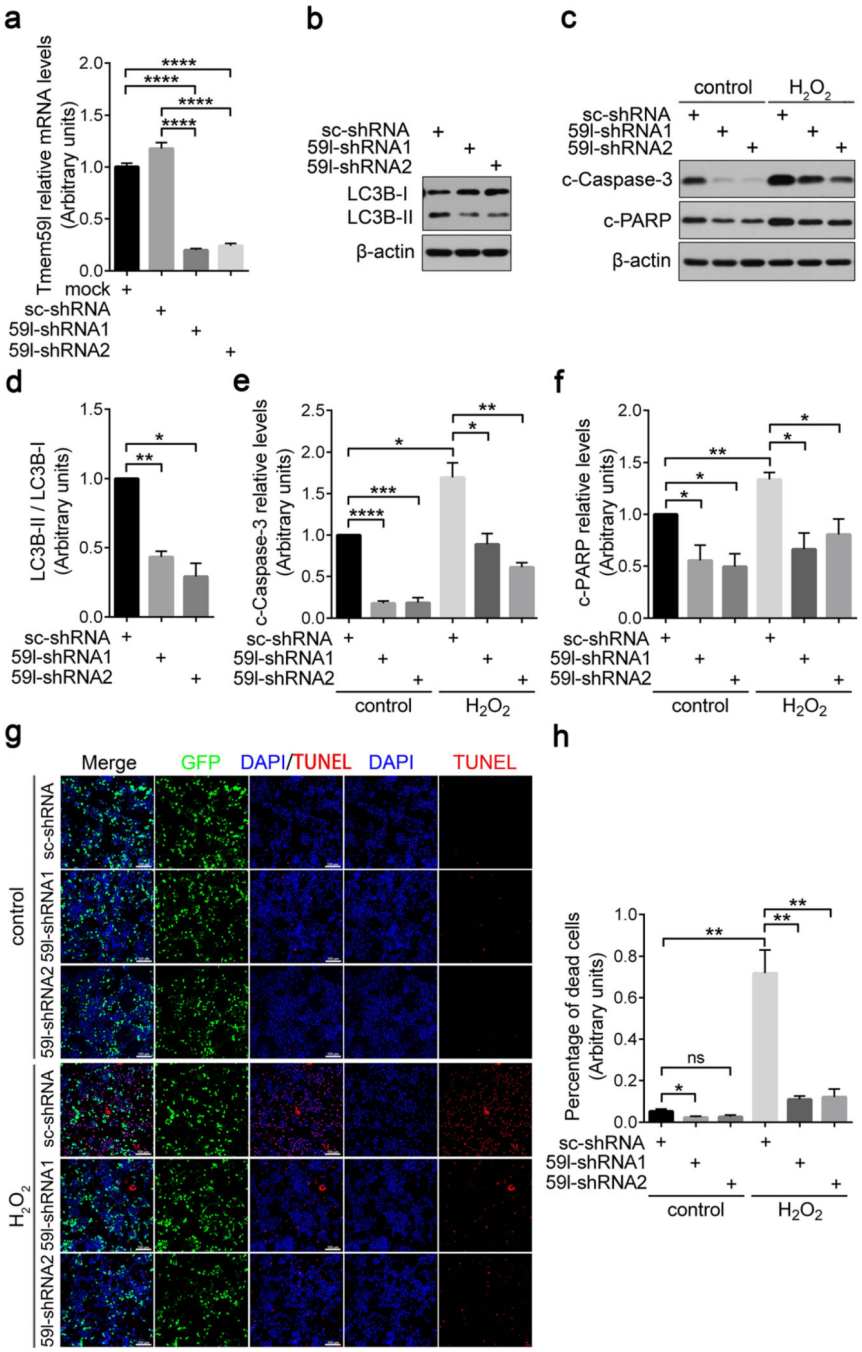

Fig. 4.

Downregulation of TMEM59L ameliorates N2a cell apoptosis induced by hydrogen peroxide insult. **a, b, d** *Tmem59l*-shRNA1, *Tmem59l*-shRNA2, or scrambled shRNA (sc-shRNA) were transfected into N2a cells for 48 h. **a** Cells were subjected to total RNA extraction, reverse transcribed, and qRT-PCR. *Tmem59l* mRNA levels were normalized to those of β-*actin* for comparison. Cells without transfection were used as a mock control. $n = 3$, ****$p < 0.0001$. **b** Equal amounts of cell lysates were subjected to Western blot analysis for LC3B-I/II. **d** LC3B-II and LC3B-I protein levels were quantified by densitometry for

comparison. $n = 3$, *$p < 0.05$, **$p < 0.01$. **c, e–h** N2a cells were transfected with *Tmem59l*-shRNA1, *Tmem59l*-shRNA2, or sc-shRNA for 43 h and then treated with 300 μM H_2O_2 or not (control) for another 5 h. **c** Equal amounts of cell lysates were subjected to Western blot analysis for c-Caspase-3 and c-PARP. **e** c-Caspase-3 and **f** c-PARP levels were quantified by densitometry for comparison. $n = 3$, *$p < 0.05$, **$p < 0.01$, ***$p < 0.001$, ****$p < 0.0001$. **g** Cells were stained by using TUNEL method and counterstained with DAPI. *Scale bars*, 100 μm. **h** TUNEL-positive cells were counted as apoptotic cells for comparison. *ns*, not significant, *$p < 0.05$, **$p < 0.01$

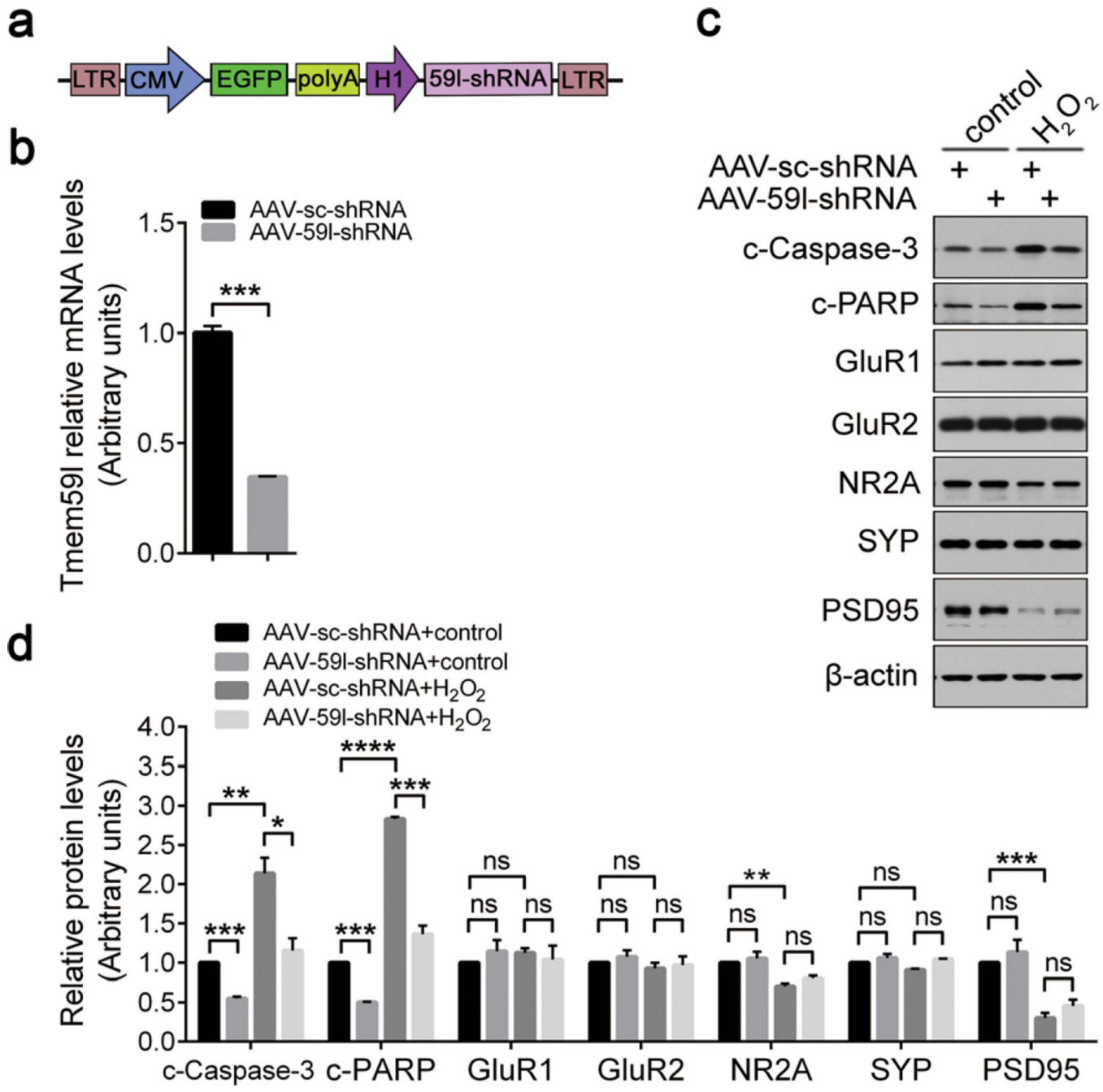

Fig. 5.

Downregulation of TMEM59L attenuates neuron apoptosis induced by hydrogen peroxide insult. **a** Schematic illustration of the AAV2/8 shRNA construct targeting mouse *Tmem59l*. **b** Primary cortical neurons were infected with AAV-59l-shRNA or AAV-sc-shRNA for 7 days at day 3 in vitro (DIV3). Total RNAs were extracted, reverse transcribed, and subjected to qRT-PCR. The mRNA levels of *Tmem59l* were normalized to those of β-*actin* and compared to that of control (set as one arbitrary unit). $n = 3$, ***$p < 0.001$. **c, d** Primary cortical neurons were infected with AAV-59l-shRNA or AAV-sc-shRNA for 7 days at DIV3 and then treated with 300 μM H_2O_2 or not (control) for another 5 h. **c** Indicated proteins

from neuronal lysates were analyzed by Western blot and **d** quantified by densitometry for comparison. $n = 3$; *ns*, not significant, $*p < 0.05$, $**p < 0.01$, $***p < 0.001$, $****p < 0.0001$

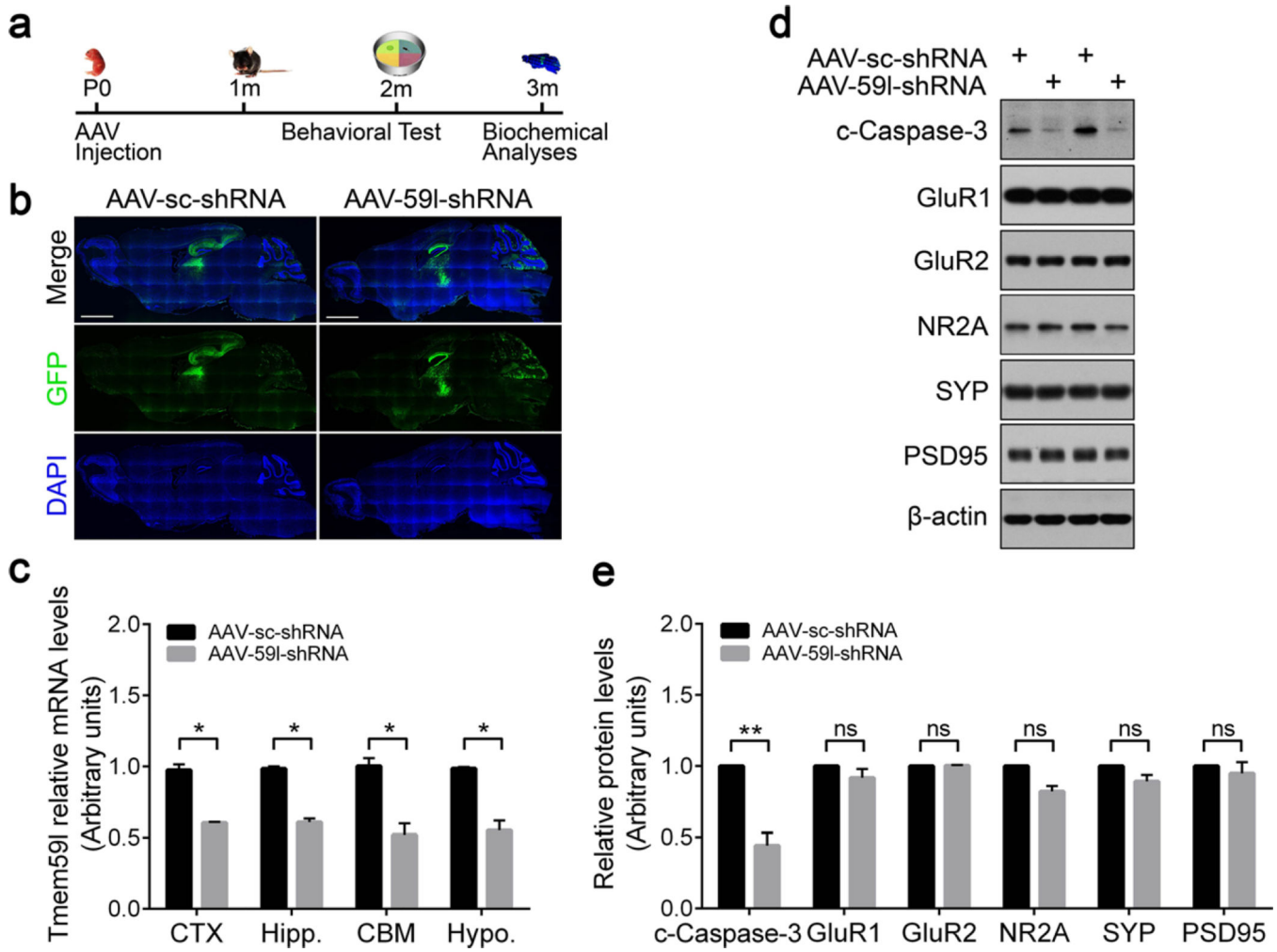

Fig. 6.

AAV-mediated knockdown of TMEM59L reduces the activation of caspase-3 in mice. **a** The workflow of stereotactic AAV injection experiment. C57BL/6 mice at P0 were bilaterally injected with AAVs expressing *Tmem59l* shRNA (*AAV-59l-shRNA*) or a scrambled shRNA (*AAV-sc-shRNA*) into the cerebral ventricle. Mice were then subjected to behavioral analyses at 2 m of age and sacrificed at 3 m of age for biochemical analyses. **b** Representative EGFP fluorescence images of whole mouse brain sections after AAV injection. *Scale bar*, 2000 μm. **c** Total RNAs were extracted from cerebral cortex (*CTX*), hippocampus (*Hipp.*), cerebellum (*CBM*), and hypothalamus (*Hypo.*) regions of mice injected with AAV for 3 months, reverse transcribed, and then subjected to qRT-PCR. The mRNA levels of *Tmem59l* were normalized to those of β-*actin* and compared to those of controls (set as one arbitrary units). $n = 4$, $^{*}p < 0.05$. **d** Indicated proteins from hippocampus lysates were analyzed by Western blot and **e** quantified by densitometry for comparison. $n = 4$; *ns*, not significant, $^{**}p < 0.01$

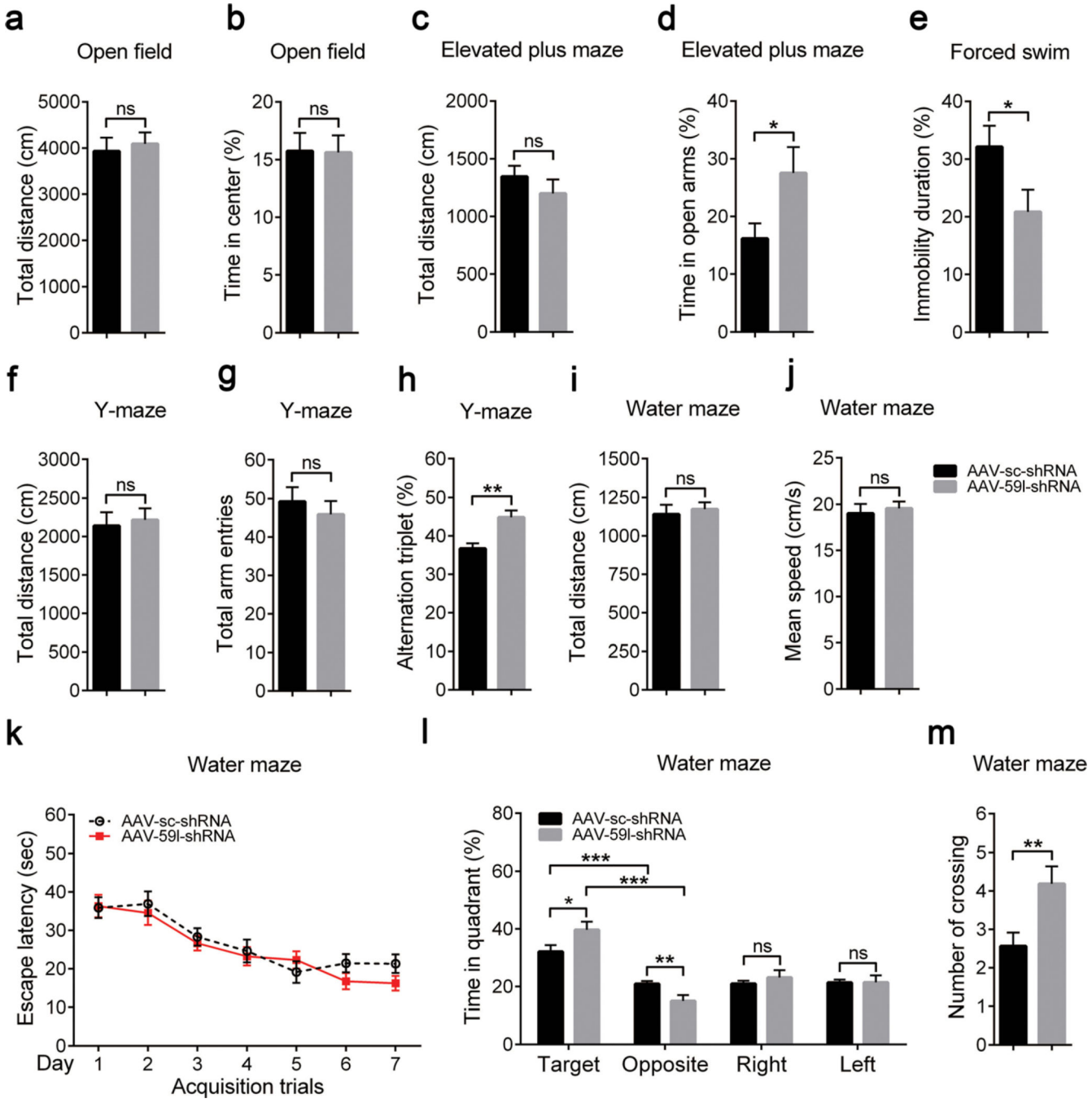

Fig. 7.

Knockdown of TMEM59L reduces anxiety- and depressive-like behaviors and enhances memory in mice. Mice injected with AAV-sc-shRNA (n = 16) and AAV-59l-shRNA (n = 16) were subjected to open field test to determine **a** total distance (cm) and **b** percentage time spent in the center region, elevated plus maze test to determine **c** total distance (cm) and **d** percentage time spent in open arms, forced swim test to determine **e** percentage immobility time, Y-maze test to determine **f** total distance (cm), **g** total arm entries and **h** percentage alternation triplet, and Morris water maze test to determine **i** total distance (cm), **j** mean

swimming speed (cm/s), **k** escape latency (s) over 7 testing days, and **l** percentage time in quadrants and **m** the number of crosses over the platform region during the probe test. *ns*, not significant, *$p < 0.05$, **$p < 0.01$, ***$p < 0.001$